Sonic Boom Theory: Its Status in Prediction and Minimization

Christine M. Darden*
NASA Langley Research Center, Hampton, Va.

This paper gives a brief review of the currently accepted understanding of sonic boom phenomena and describes the manner in which modified linearized theory and geometric acoustics are used to predict the sonic boom caused by a complex aircraft configuration. Minimization methods that have evolved in recent years are discussed, with particular attention given to a method developed by Seebass and George for an isothermal atmosphere which was modified for the real atmosphere by Darden. An additional modification which permits the relaxation of the nose bluntness requirement in the defining aircraft also is discussed. Finally, an overview of current areas of sonic boom research is given.

I. Introduction

THE ban of supersonic flight over the continental U. S. and the associated economic penalties played a major role in the demise of our national SST program a few years ago. With the impending scheduled flights of the Concorde and then the TU144, the position of the United States in the worldwide aeronautical community is threatened.

The sonic boom, which was the primary cause of the ban on supersonic flight over the continental U. S., has undergone considerable investigation by scientists and engineers alike within the past two decades. The ultimate goal of this research has been to develop an understanding of how sonic booms are generated, to develop methods of predicting sonic booms, and, finally, to develop means of reducing the sonic boom so that overland supersonic flight will be made possible.

Today, knowledge of sonic boom phenomena is quite advanced and the theoretical methods that have been developed for predicting the sonic boom are generally accepted as giving valid results at flight altitudes for Mach numbers up to about 3. Attention in recent years has been given to ways of reducing the sonic boom by using the existing knowledge of how it is generated. This paper will review the currently accepted understanding of sonic boom phenomena, will outline prediction theories and minimization methods that have evolved in recent years, will discuss drag penalties and tradeoffs associated with low boom configurations, and will mention areas of current research.

II. Sonic Boom Phenomena

Pressure disturbances created by an airplane in flight travel in all directions at the local speed of sound. When the aircraft itself is flying faster than the speed of sound, it will advance faster than the disturbances it has generated, creating a conical region which extends behind the aircraft nose and defines the entire region of disturbance at any given time. This conical region is shown schematically in Fig. 1. The intersection of this region with the ground defines a so-called "footprint" of pressure disturbances. Pressure signals felt within the footprint region normally display the characteristics illustrated in the pressure signature diagram in the left upper corner of Fig. 1. Initially, there is an instantaneous rise in the pressure caused by the shock from the aircraft nose. After the initial shock, there is a linear decline in the pressure to below the normal level, and then there occurs another shock which restores the pressure to its normal value. It is these shocks which are heard by the ground observer. The level of Δp in the pressure signature indicates the loudness of the boom that will be heard. If the time between these two shocks is very short, the observer will hear only one boom, but as the time between the shocks increases, the observer is more likely to hear two booms in rapid succession. On the other hand, the level of indoor disturbance or structural damage attributed to the pressure signature is believed to be more dependent on the impulse (the integral of the positive portion) and the length of the signature.

Referring again to the region of ground disturbance, notice that, as indicated by the inserted signatures, the loudest boom occurs on the ground track and the signature gets longer and the boom weaker as the distance from the ground track of the aircraft increases. This region of pressure disturbance can be 60 to 70 miles wide, depending on the altitude and Mach number of the aircraft.

III. Prediction Methods

Predictions of the sonic boom levels caused by complex supersonic aircraft configurations are based on work done by Whitham[1] for axisymmetric supersonic projectiles and by Walkden,[2] who extended the theory to wing-body lifting configurations by representing these as bodies of revolution. The most widely used prediction methods today make use of the linearized theory supersonic area rule developed by

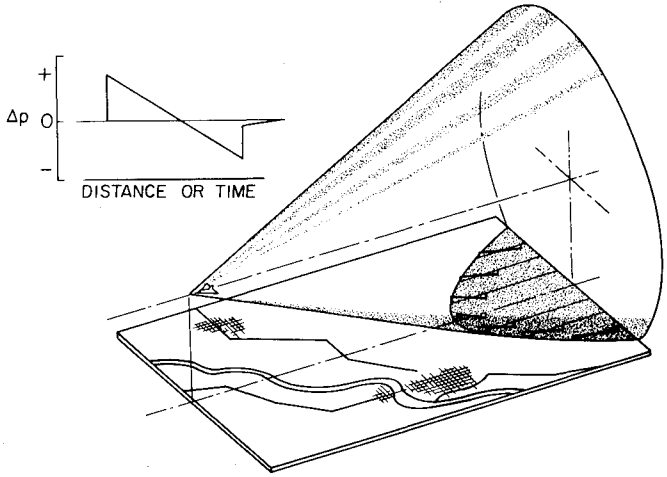

Fig. 1 Mach cone of pressure disturbances.

Presented as Paper 76-1 at the AIAA 14th Aerospace Sciences Meeting, Washington, D. C., Jan. 26-28, 1976; submitted Feb. 4, 1976; revision received Aug. 25, 1976.

Index categories: Aeroacoustics; Noise.

*Aerospace Engineer, High-Speed Aerodynamics Division. Member AIAA.

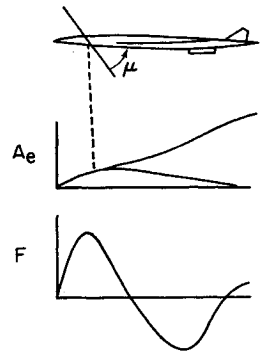

Fig. 2 Prediction methods.

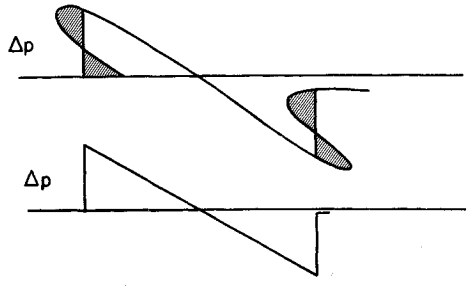

Hayes.[3] At large distances, the Mach fore cone can be treated as a plane in which all disturbances in that plane arrive at an observer simultaneously. Thus, one can determine a linear distribution of singularities that produce the same pressure disturbances at large distances as those produced by the aircraft. This linear source-sink distribution can be related to an equivalent body area distribution made up of volume and lift contributions. The normal projections of area intercepted by the Mach cutting planes define the equivalent body area due to volume as shown in Fig. 2, and the area due to lift is determined by integrating the lifting forces up to the Mach cut. The equivalent area distribution then defines the Whitham "F function" through the following relations:

$$F(x) = \frac{1}{2\pi}\int_0^x \frac{A_e''}{(x-t)}\,dt$$

This function represents the source and influence distribution which causes the same disturbances as the aircraft at large distances from the aircraft. A typical equivalent area distribution and F function are shown in Fig. 2.

Because the pressure signal propagates at the local speed of sound, and each point of the signal advances according to its amplitude, the signal is distorted at the ground and theoretically could be multivalued. The physically unrealistic multiple values of pressure in the ground signal are, however, eliminated by the introduction of shocks. Shock location, based on the observation that for weak disturbances the shock bisects the angle between two merging characteristic lines, is determined by a balancing of the signature areas within loops on either side of the shocks. This procedure is demonstrated by the shaded areas of the distorted signal in Fig. 2. For present-day supersonic aircraft, the distance of propagation and the pattern of shock coalescence has been such that, at ground level, only two shocks remain in the signature with a linear variation of pressure between them as seen in Fig. 3 – thus the name "far-field N wave."[4] For the far-field N wave, the shape of the generating aircraft has an effect on the magnitude but no effect on the shape of the resulting signature. Based on the assumption that all pressure signatures reaching the ground would have the characteristic N-wave form, Jones showed that the lower bound for the shocks occurred when the defining area distribution was extremely blunt and the corresponding F function was characterized by a Delta function at $x=0$.[5,6] Shape changes required in current aircraft to produce such equivalent areas were found to result in great efficiency losses because of drag penalties.[7]

It was observed by McLean[8] that attention should not be confined solely to the far-field signature, because, during transonic acceleration, the signature created by large and slender SST's might not necessarily attain their far-field N waveform. During the mid 1960's, as more and more researchers began to look at ways of reducing boom levels, it was observed that even in cruise conditions, a sufficiently long airplane could produce a signature which has not attained its N waveform. Further along this avenue of thought, Hayes[9] pointed out that in the real atmosphere, characteristics coalesce more slowly than in the uniform atmosphere on which previous estimates of near-field characteristics were based, and the shape of the signature "freezes," thus increasing the possibility that midfield signature shapes may reach the ground.

Because the shape of a midfield wave indeed does depend on the shape of the aircraft, such shaping was recognized as a much more powerful means of reducing the sonic boom than previously believed. Seebass[10] and George,[11] on extending the work of McLean, showed that the lower bounds for the bow shock of these midfield signatures also required the F function to be characterized by a Delta function at $x=0$.

The form of the F function for minimizing the bow shock strength in midfield signatures and the observation that the effective length available for bow shock minimization is reduced when the rear shock also is constrained led to the F function deduced by Seebass and George in their minimization of the entire signature.[12,13] That this was the minimizing F function was shown by Lung,[14] using bang-bang control theory. The scheme developed by Seebas and George which placed constraints on both the bow and rear shocks, and produced either the minimum shock or minimum overpressure signature were applied to propagation through an isothermal atmosphere. As with other minimization techniques, these minimum booms were found to be produced by F functions characterized by a Delta function, or, equivalently, by effective area distributions having an infinite

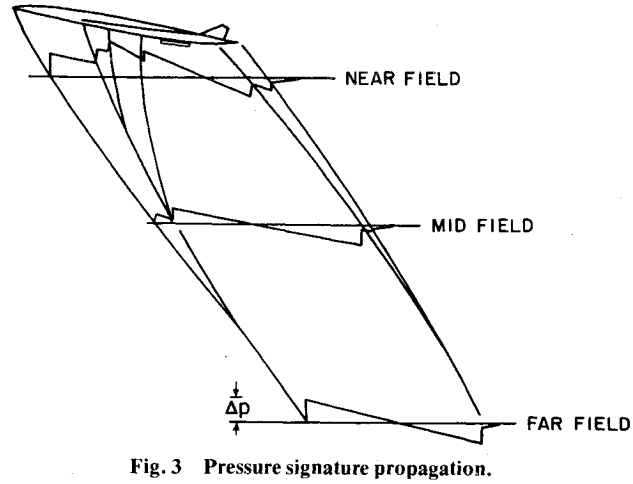

Fig. 3 Pressure signature propagation.

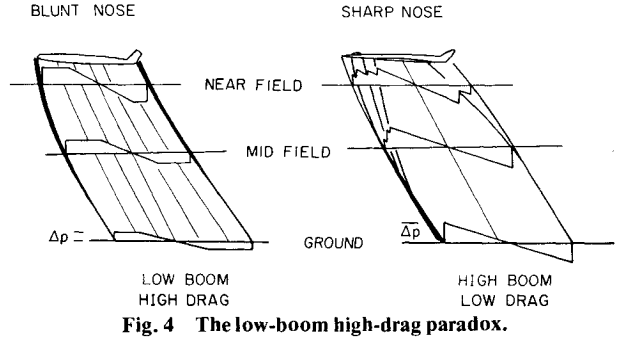

Fig. 4 The low-boom high-drag paradox.

gradient at the nose. The design of aircraft to match these area distributions generally result in nose shapes so blunt as to create substantial penalties. This result, although, seemingly paradoxical, can be explained by the created shock attenuation pattern in which the shock strengths, and therefore the drag, are found to be greatest near the aircraft with no further shocks forming during the propagation of the wave front as illustrated in Fig. 4. The net result of this process is weaker shocks at large distances because of attenuation, but an overall increase in drag. In contrast, notice that the shocks and drag are weaker at the sharp-nosed aircraft, but that coalescence of shocks causes a much stronger shock at mid- and far-field distances. If an aircraft configuration is to incorporate boom minimization features and not suffer aerodynamic penalties which inordinately affect its flight efficiency, range, payload, productivity, and so forth, then means must be provided for conducting nose bluntness sensitivity studies in design tradeoffs.

IV. Sonic Boom Minimization with Nose Bluntness Relaxation

The following is a brief description of the Seebass-George minimization scheme with modifications to provide propagation through the real atmosphere[15] and control over the bluntness of the area distribution and thereby the drag of the configuration. The assumed form of the minimizing F function is shown in Fig. 5. In mathematical terms it may be expressed as

$$F(y)=2xH/y_f \qquad (0\le x\le y_f/2) \qquad (1a)$$

$$F(y)=C(2x/y_f-1)-H(2x/y_f-2) \qquad (y_f/2\le x<y_f) \qquad (1b)$$

$$F(y)=B(x-y_f)+C \qquad (y_f\le x<\lambda) \qquad (1c)$$

$$F(y)=B(x-y_f)-D \qquad (\lambda\le x\le l) \qquad (1d)$$

In these equations H, B, C, D, and λ are unknown coefficients which are determined by the cruise conditions of the aircraft, by nose length, by the prescribed ratio of bow to rear shock, and by the parameter of the signature which is being minimized. Recall that the Whitham function $F(y)$ represents the shape characteristics of the pressure signature and is defined in Ref. 1 in terms of the equivalent area distribution

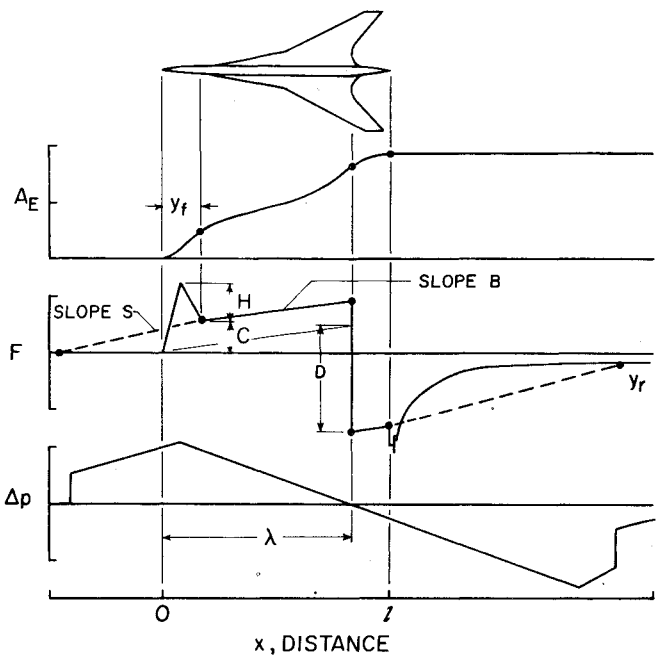

Fig. 5 Illustration of near-field sonic boom theoretical concepts.

as

$$F(y)=\frac{1}{2\pi}\int_0^y \frac{A_{e''}}{(y-x)^{1/2}}dx \qquad (2)$$

Crucial to this minimization technique is the fact that Eq. (2) is an Abel integral equation which may be inverted to give the function $A_e(x)$ in terms of the F function. When this function is evaluated at l, the result is

$$A_e(l)=4\int_0^l F(y)\,(l-y)^{1/2}dy \qquad (3)$$

Upon substituting the minimizing form of the F function into Eq. (3) and integrating, the following equation for the development of cross-sectional area is obtained:

$$\begin{aligned}A_e(x)=&\frac{32}{15}\frac{H}{y_f}x^{5/2}+1(x-y_f/2)\frac{8}{15}(x-y_f/2)^{3/2}\\&\{(3y_f/2+2x)(1/y_f)(2C-4H)+5(2H-C)\}\\&+1(x-y_f)4(x-y_f)^{3/2}\\&\{(2C/y_f)\left(-\frac{2}{15}\right)(3y_f+2x)+\frac{2}{3}C\\&+\frac{4}{15}(H/y_f)(3y_f+2x)-\frac{4}{3}H\\&+\frac{2}{15}B(3y_f+2x)-\frac{2}{3}By_f+\frac{2}{3}C\}\\&-1(x-\lambda)\frac{8}{3}(x-\lambda)^{3/2}(C+D)\end{aligned} \qquad (4)$$

where $1(x-\alpha)$ is the Heaviside Unit step function. A typical form of the resulting area distribution is seen in Fig. 5.

If the effects of aircraft wake and engine exhaust are neglected, and, if the aircraft cross-sectional area is zero at its base, then the area at l is entirely due to cruise lift or

$$\begin{aligned}A_e(l)=\frac{\beta w}{\rho U^2}=&\frac{32}{15}\frac{H}{y_f}l^{5/2}+\frac{8}{15}(l-y_f/2)^{3/2}\\&\{(3y_f/2+2l)\left(\frac{1}{y_f}\right)(2C-4H)+5(2H-C)\}\\&+4(l-y_f)^{3/2}\{(2C/y_f)-\frac{2}{15}(3y_f+2l)\\&+\frac{2}{3}C+\frac{4}{15}(H/y_f)(3y_f+2l)-\frac{4}{3}H+\frac{2}{15}B(3y_f+2l)\\&-\frac{2}{3}By_f+\frac{2}{3}C\}-\frac{8}{3}(l-\lambda)^{3/2}(C+D)\end{aligned} \qquad (5)$$

The first constraint imposed upon $F(y)$ is that the front area balance must occur at $y=y_f$, where y_f is the first point at which $F(y)=C$, that is,

$$\int_0^{y_f} F(y)\,dy=G=\frac{\alpha_{y_f}}{2}F(y_f)=\frac{\alpha_{y_f}}{2}C \qquad (6)$$

For the real atmosphere, the advance[16] of any point of the signal is given by

$$\alpha_y=\frac{\Gamma M_h{}^3F(y)}{(2\beta)^{1/2}}\int_0^z \frac{p_{a,h}}{p_a}\left(\frac{\rho a_h}{\rho_h a}\right)^{1/2}\left(\frac{A_h}{z_h A}\right)^{1/2}\frac{M}{\beta}dz \qquad (7)$$

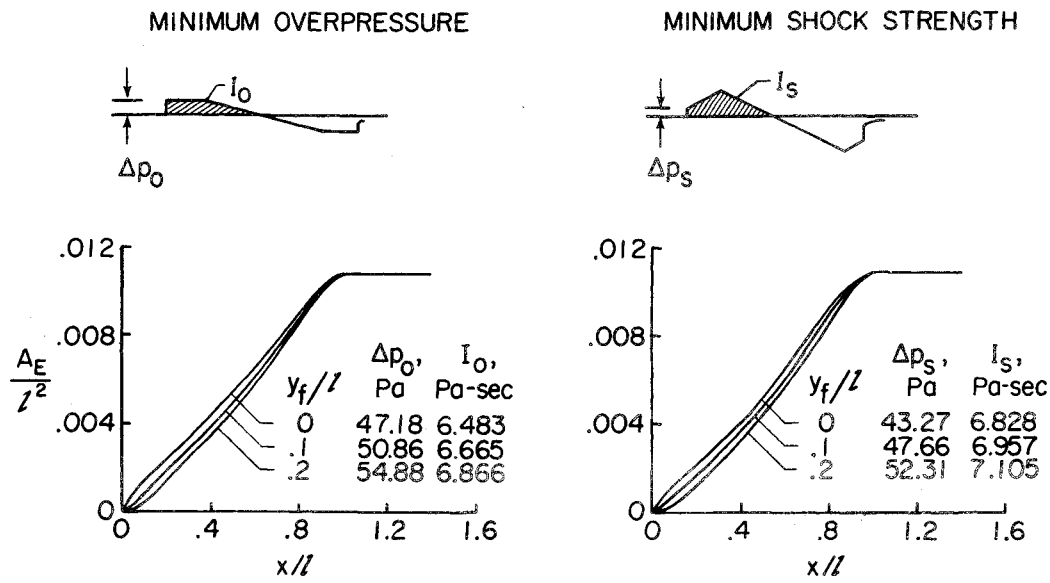

Fig. 6 Typical equivalent area distribution requirements for minimization of overpressure and of shock strength: $M=2.7$; $w=272{,}155$ kg (600,000 lb); $h=18{,}288$ m (600,000 ft); $l=91.44$ m (300 ft).

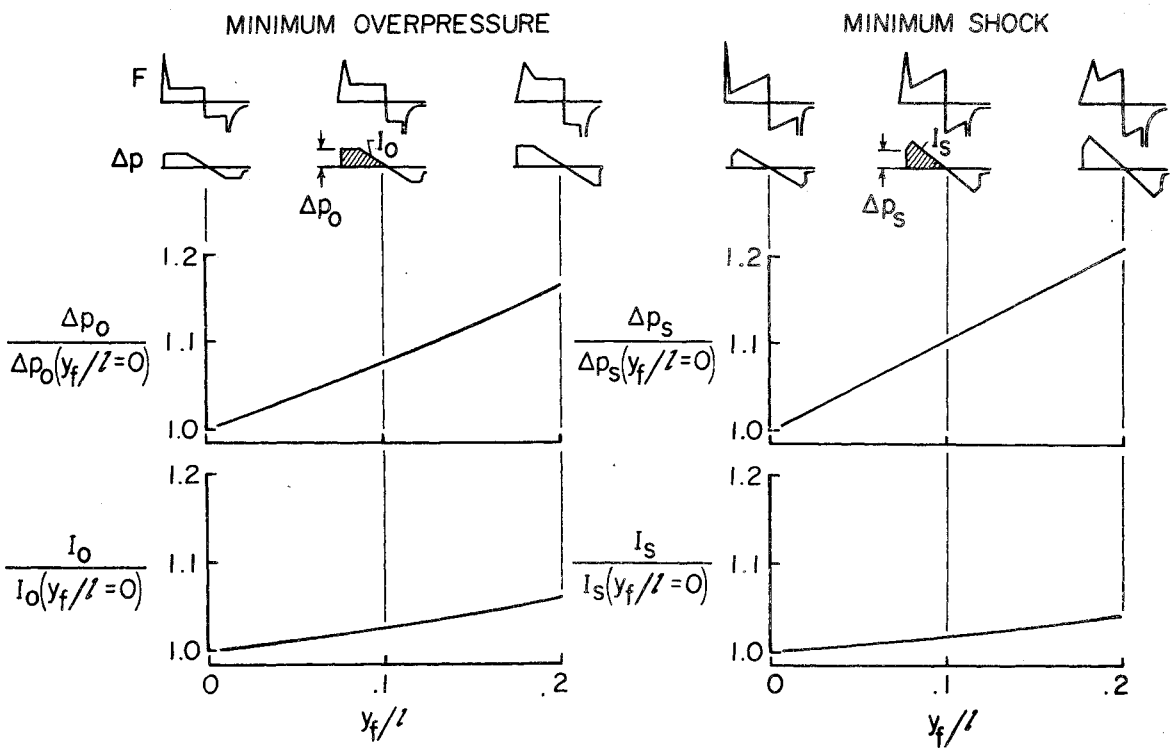

Fig. 7 Variation of shock strength and impulse with nose length y_f: $M=2.7$; $h=18{,}288$ m (60,000 ft); $w=272{,}155$ kg (600,000 lb); $l=91.44$ m (300 ft).

where z is the vertical distance of the signal from the aircraft axis, z_h is the vertical distance of the initial waveform from the aircraft axis, A and A_h are ray tube areas determined from

$$\frac{A_h}{z_h A}=\left\{M_h\left[1-\frac{1}{M(z)^2}\right]^{1/2}\int_0^z \frac{dz}{[M(z)^2-1]^{1/2}}\right\}^{-1} \tag{8}$$

and $\Gamma=(\gamma+1)/2$. The initial waveform must be defined away from the aircraft, because the F function only can represent the body shape accurately at several body lengths away, and the acoustical theory used in describing the propagation of the signal fails near the aircraft. The slope of the balancing line is proportional to the reciprocal of the advance at any point of the signal, thus

$$s=\frac{(2\beta)^{1/2}}{\Gamma M_h^{3}\int_0^{h}\frac{p_{a,h}}{p_a}\left(\frac{\rho a_h}{\rho_h a}\right)^{1/2}\left(\frac{A_h}{z_h A}\right)^{1/2}\frac{M}{\beta}\,dz}=\frac{F(y)}{\alpha(y)} \tag{9}$$

For the rear area balancing to occur between points l and y_r then

$$\int_l^{y_r} F(y)\,dy=\tfrac{1}{2}[(Bl-D+F(y_r)](y_r-l) \tag{10}$$

where y_r is the unknown second intersection point of the rear area balancing line with $F(y)$. If a cylindrical wake is assumed, $F(y)$ and its integral for $y>l$ can be expressed in

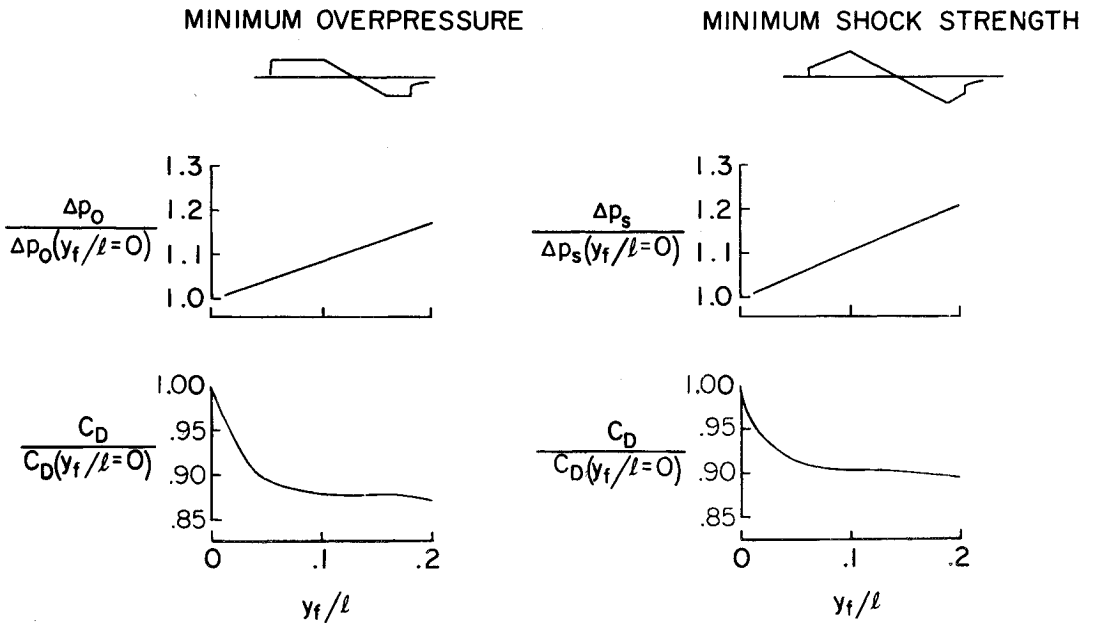

Fig. 8 Estimated drag increments associated with configuration changes for sonic boom minimization: $M=2.7$; $h=18{,}288$ m (60,000 ft); $w=272{,}155$ kg (600,000 lb).

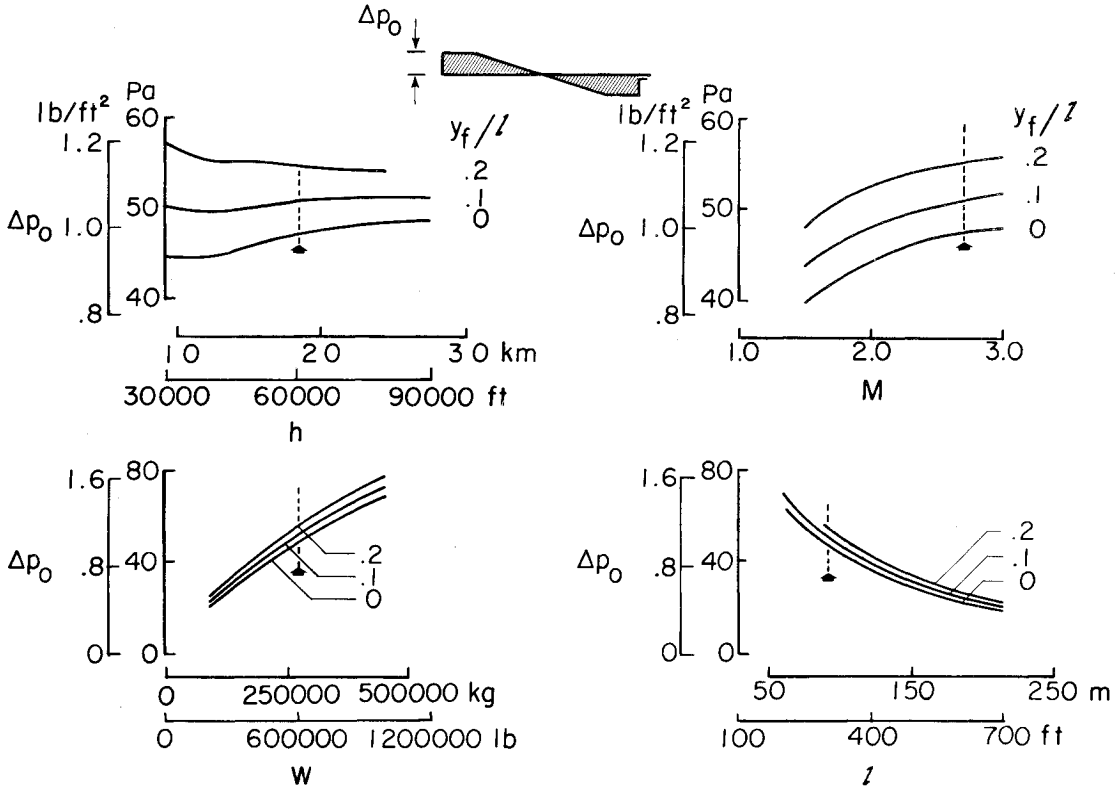

Fig. 9 Variation of minimum overpressure with some of the significant size and flight condition variables. Normal conditions indicated by the arrows.

terms of $F(y)$ for $y<l$ according to Ref. 17 as follows:

$$F(y) = -\frac{l}{\pi(y-l)^{1/2}}\int_0^l \frac{(l-x)^{1/2}}{y-x}F(x)\,dx \quad (y>l) \tag{11}$$

$$\int_l^{y_r} F(y)\,dy = -\frac{2}{\pi}\int_0^l F(x)\tan^{-1}\left(\frac{y_r-l}{l-x}\right)^{1/2}dx \quad (y>l) \tag{12}$$

It is necessary to define $F(y)$ and its integral for $y>l$ in this way for optimization problems, since aircraft geometry and thus the Whitham function can be varied arbitrarily only in the range $0\le y\le l$. The constraint on the ratio of shocks is given by

$$\frac{p_f}{p_r} = \frac{C}{D-B(l-y_f)+F(y_r)} \tag{13}$$

To insure that y_r is an intersection point of $F(y)$ and the balancing line, then

$$F(y_r) = s(y_r-l)+B(l-y_f)-D \tag{14}$$

and the slope of $F(y)$ at y_r must be less than s.

Solving the system of Eqs. (5, 6, 10, 13, and 14) provides values for the constants H, C, D, λ, and y_r. Types of signatures studied include flat-topped signatures in which overpressure is minimized with $B=0$ and signatures in which $F(y)$ is allowed to rise between y_f and λ with a resulting minimum shock followed by a pressure rise as illustrated in Fig. 5. The value of B in this form of $F(y)$ may range between 0 and s. One difficulty of this minimization approach is that, as yet, there is no precise definition of the rise time that will allow the ear to detect only the bow shock and not be sensitive to the peak as well. With the values of the coefficients known, the minimizing F function and area distributions may be determined by Eqs. (1) and (4).

To convert $F(y)$ into pressure near the airplane, the following equation is used

$$\left(\frac{P}{p_a}\right)_h = \frac{\gamma M^2 F}{(2\beta z_h)^{1/2}} \tag{15}$$

and on the ground

$$P_g = \left(\frac{A_h}{A_g}\right)^{1/2}\left(\frac{\rho_g a_g}{\rho_h a_h}\right)^{1/2} P_h \tag{16}$$

Finally, by using a ground reflection factor k, the pressure perturbations are converted into the ground signature by

$$\Delta p_g = P_g k \tag{17}$$

The ground level signature is represented by the signature shown in the lower portion of Fig. 5. This minimization procedure has been programmed for digital computers with the required inputs being nose length, y_f, and the flight conditions of Mach number, altitude, equivalent length, and weight.

V. Typical Applications of the Method

Except where otherwise indicated, all of the results shown are for the following conditions: Mach number, 2.7; altitude, 18,288 m (60,000 ft); weight, 272,155 kg (600,000 lb); equivalent length, 91.44 m (300 ft); reflection factor, 2.0; ratio of bow to rear shock pressure, 1; and $B=0.5$ s. The value of the front balancing point yf determines the length of the conical nose region of the equivalent area distribution and is the controlling factor for drag when all of the other flight conditions remain constant. Referring again to Fig. 5, this position is indicated on the F function and the corresponding area distribution.

The effect that varying y_f has on the equivalent area distributions for both the minimum overpressure and minimum shock signatures is seen in Fig. 6. Each of the distributions was determined from the inversion formula which defines the effective area corresponding to the minimizing F function for a given value of y_f. Values of the overpressure and impulse which correspond to these distributions have been inserted for reference. Recall that the impulse is the integral of the positive portion of the pressure signature, as indicated in the signatures at the top of Fig. 6. Note that the lowest values of overpressure and impulse for these conditions occur when the area distribution has an infinite gradient at the nose. As y_f increases, the longer conical nose region, generated to reduce drag, also causes an increase in overpressure and impulse. Because of this, extensive tradeoff studies between drag and boom levels would be necessary in any aircraft design studies. The ratio of this increase for both types of signatures as a function of nose lengths ratio is seen more easily in Fig. 7. With increasing values of y_f, note that the area under the peak portion of the F function also increases but not in the same proportions. Therefore, to achieve the necessary total area, the level of the constant portion of the F function also must increase, thereby producing a higher level of Δp and impulse. For illustrative purposes, the nose spike of the F function for $y_f=0$ has been drawn with a finite width. For this condition, the spike is defined mathematically as a pulse of zero width and infinite height which nevertheless has a finite area. Δp in these figures is the level of overpressure at the bow shock and represents the initial "bang" heard by the ear when a sonic boom occurs.

The variation of overpressure level with the corresponding drag levels is seen in Fig. 8. To develop the corresponding variation of drag with y_f, since at this point configurations to

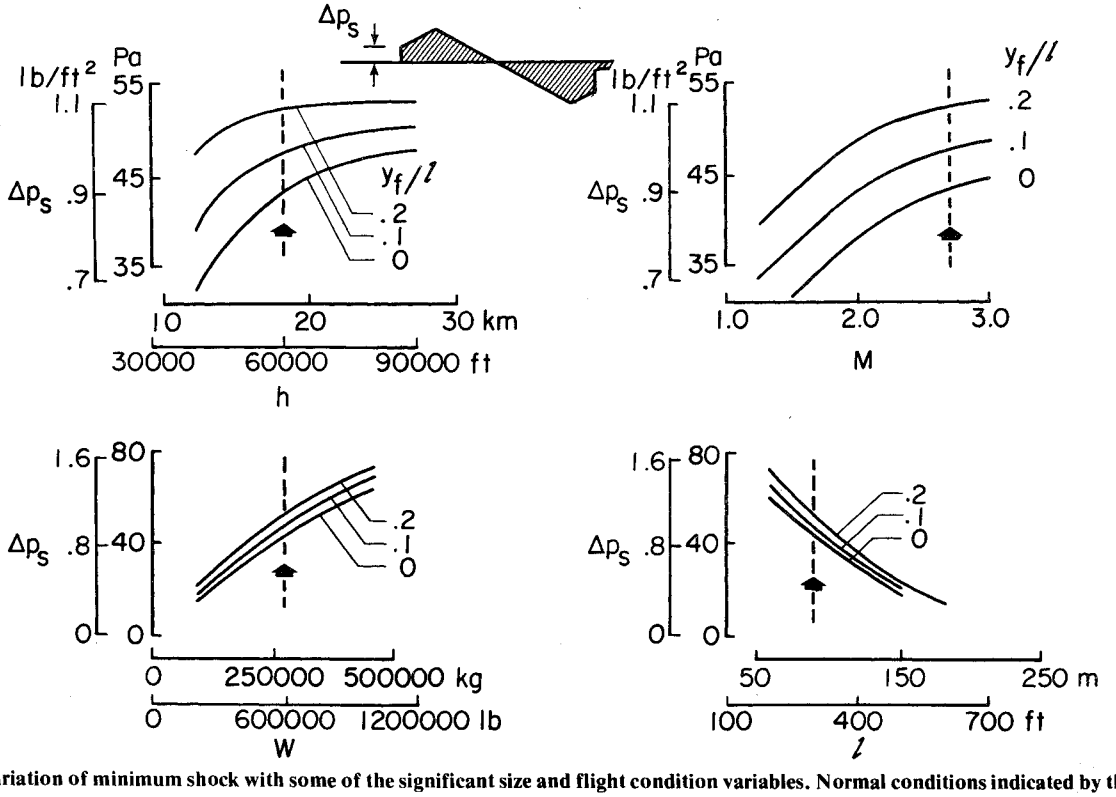

Fig. 10 Variation of minimum shock with some of the significant size and flight condition variables. Normal conditions indicated by the arrows.

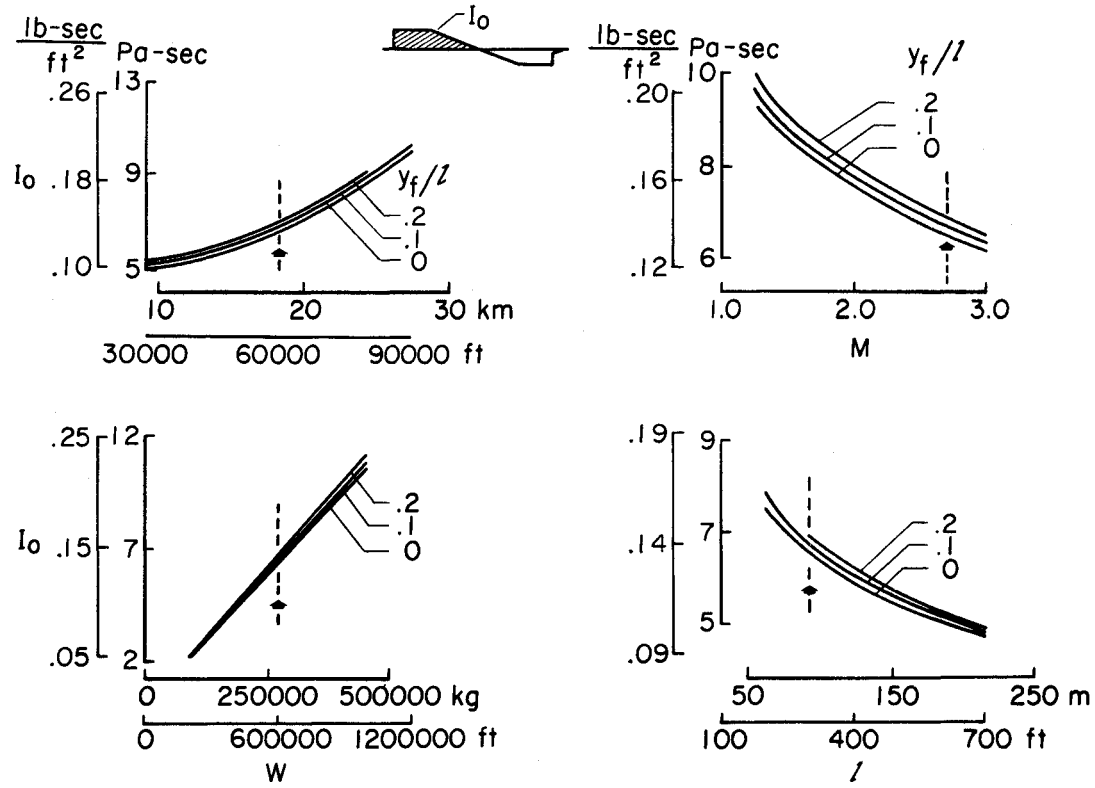

Fig. 11 Variations of impulse in minimum overpressure signatures with some of the significant size and flight condition variables. Normal conditions indicated by the arrows.

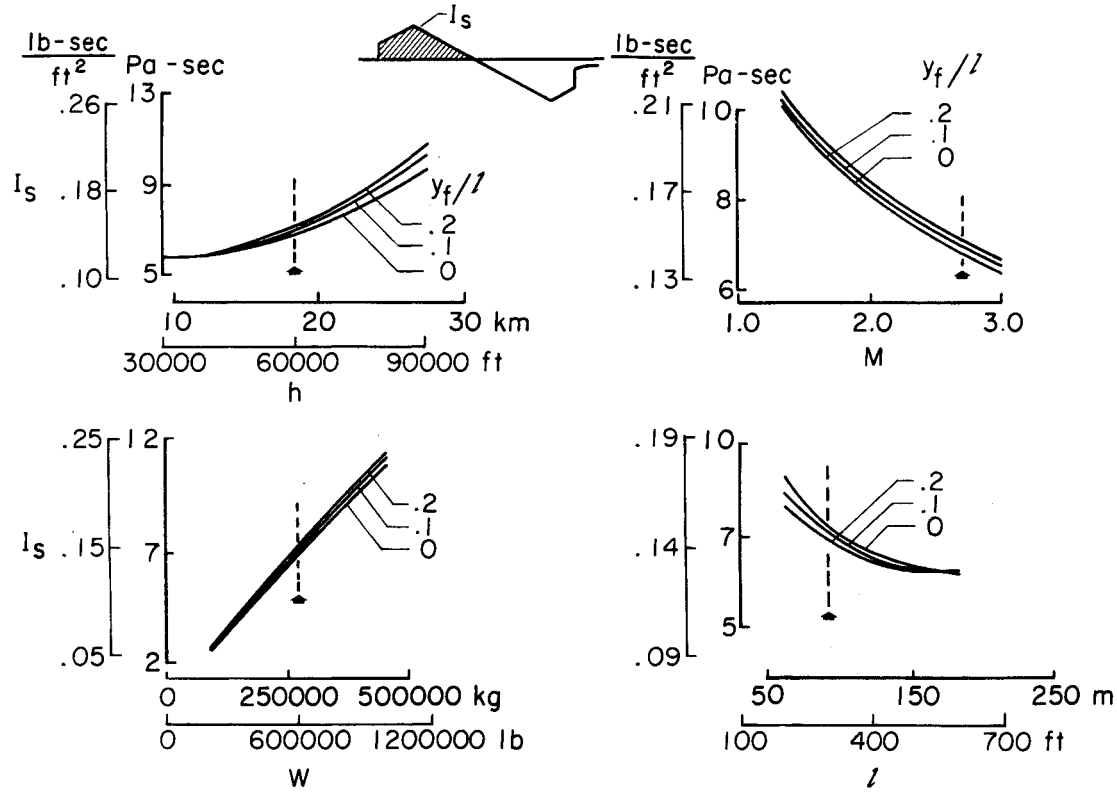

Fig. 12 Variations of impulse in minimum shock signatures with some of the significant size and flight condition variables. Normal conditions indicated by the arrows.

match these areas have not been defined, the assumption is made that necessary configuration changes would be confined to the fuselage forebody itself. The increment in drag produced by these changes then was applied to drag values for a typical arrow-wing SST configuration. As seen in Fig. 8, there is a sharp decline in drag as the blunt nose is converted to a conical region. Thus, one could expect in design tradeoff studies to significantly reduce the boom and yet not suffer prohibitive drag penalties by defining the proper nose length ratio.

The actual trend of overpressure with flight conditions of Mach number, weight, length, and altitude is seen in Fig. 9. The minimum curve in each figure represents the $y_f = 0$ case, with the higher ones representing y_f/l of 0.1 and 0.2, respectively. The variation of shock for the minimum shock signatures for the same flight parameters is seen in Fig. 10. Recall that in these signatures there is an increase in overpressure following the initial shock.

The variation of impulse with the flight conditions is seen in Fig. 11 for the minimum overpressure signature at the three ratios of y_f/l. This same variation for the minimum shock signature is shown in Fig. 12.

Many of the results shown in Figs. 9-12 for $y_f/l = 0$ have been shown for the isothermal atmosphere in Ref. 13. Although the isothermal predictions of Δp are quite good at moderate supersonic Mach numbers, care must be exercised in evaluating the impulse results and in using the corresponding area distributions. A more detailed comparison of results from the two atmospheres may be found in Ref. 15.

Evidence has not indicated clearly which of the parameters shown should be minimized in the pressure signature. There yet may be found some combination of these which must be minimized to achieve an acceptable level of the pressure signature. If so, the principles and experiences developed for minimizing the overpressure or the shock level should be applicable to some other defining parameter.

VI. Active Research Areas and Areas for Further Study

Because past propagation theories required pressure disturbances to be defined several body lengths away from the aircraft, sonic boom wind-tunnel test models have had to be constructed so small that incorporation of the detailed camber and twist distributions needed to achieve the proper area distributions have not been possible. Current work by Ferri et al. to develop a propagation method based on the three-dimensional method of characteristics which would accept as input the fully developed flowfield about an airplane configuration would serve to alleviate this problem. This method, which includes nonlinear effects and entropy and enthalpy variations, also will be applicable in the hypersonic speed regime where current theories are not valid.[18]

Aircraft maneuvers and accelerations often will cause a focus of rays from the aircraft, producing a phenomenon known as the "caustic" or "superboom." Current efforts in the area of caustics are discussed in Refs. 19 and 20. Studies of atmospheric effects on booms and additional studies of the effects of the sonic boom on humans, animals, and structures also are being conducted at the University of Toronto Institute for Aerospace Studies.[20]

The idea of "boom-constrained" design has introduced into design studies problems heretofore not present. There is a need for inverse design methods which design lifting surfaces and volumes to match given lift and volume distributions. In addition to this and the need for higher-order, more exact theories, there is a need for more experimental results based on the minimization theories that have been advanced thus far. Such a test program is being planned at Langley within the next few months.

VII. Concluding Remarks

A brief review of the current understanding of the phenomenon known as sonic boom has been given, and methods currently used to predict the sonic boom created by a given aircraft configuration have been described. In addition, a minimization scheme based on that of Seebass and George which provides a tool for tradeoffs between drag and boom levels in design studies has been outlined. Finally, areas of current efforts in sonic boom research and areas needing further study have been mentioned.

References

[1]Whitham, C. B., "The Flow Pattern of a Supersonic Projectile," *Communications in Pure and Applied Mathematics*, Vol. V, Aug. 1952, pp. 301-348.

[2]Walkden, F., "The Shock Pattern of a Wing-Body Combination Far From the Flight Path," *Aeronautical Quarterly*, Vol. 9, May 1958, pp. 164-194.

[3]Hayes, W. D., "Linearized Supersonic Flow," Thesis, California Institute of Technology, 1947; reprinted as North American Aviation Rept. AL-222.

[4]Carlson, H. W. and Maglieri, D. J., "Review of Sonic Boom Generation Theory and Prediction Methods," *Journal of the Acoustical Society of America*, Vol. 51, 1972, pp. 675-682.

[5]Jones, L. B., "Lower Bounds for Sonic Bangs," *Journal of the Royal Aeronautical Society*, Vol. 65, June 1961, pp. 433-436.

[6]Jones, L. B., "Lower Bounds for Sonic Bangs in the Far Field," *Aeronautical Quarterly*, Vol. XVIII, Pt. 1, Feb. 1967, pp. 1-21.

[7]Carlson, H. W., "Influence of Airplane Configuration on Sonic Boom Characteristics," *Journal of Aircraft*, Vol. 1, March-April 1964, pp. 82-86.

[8]McLean, F. E., "Some Nonasymptotic Effects on Sonic Boom of Large Airplanes," NASA TN D-28777, 1965.

[9]Hayes, W. D., "Brief Review of Basic Theory," *Sonic Boom Research*, edited by A. R. Seebass, NASA SP-147, 1967, pp. 3-7.

[10]Seebass, R., "Minimum Sonic Boom Shock Strengths and Overpressure," *Nature*, Vol. 221, Feb. 1969, pp. 651-653.

[11]George, A. R., "Lower Bounds for Sonic Booms in the Mid-field," *AIAA Journal*, Vol. 7, Aug. 1969, pp. 1542-1545.

[12]George, A. R. and Seebass, R., "Sonic Boom Minimization Including Both Front and Rear Shocks," *AIAA Journal*, Vol. 9, Oct. 1971, pp. 2091-2093.

[13]Seebass, R. and George, A. R., "Sonic Boom Minimization," *Journal of the Acoustical Society of America*, Vol. 51, Pt. 3, Feb. 1972, pp. 686-694.

[14]Lung, J. L., "A Computer Program for the Design of Supersonic Aircraft to Minimize Their Sonic Boom," M.S. Thesis, Cornell University, 1975.

[15]Darden, C. M., "Minimization of Sonic Boom Parameters in the Real and Isothermal Atmosphere," NASA TN D-7842, March 1975.

[16]George, A. R. and Plotkin, K. J., "Sonic Boom Waveforms and Amplitudes in a Real Atmosphere," *AIAA Journal*, Vol. 7, Oct. 1969, pp. 1978-1981.

[17]Jones, L. B., "Lower Bounds for the Pressure Jump of the Bow Shock of a Supersonic Transport," *Aeronautical Quarterly*, Vol. XXI, Pt. 1, Feb. 1970, pp. 1-17.

[18]Ferri, A., Ting, L., and Lo, R. W., "Nonlinear Sonic Boom Analysis Including the Asymmetric Effects," AIAA Paper 76-587, Palo Alto, Calif., July 1976.

[19]Lung, J. L., Tiegerman, B., Yu, N. J., and Seebass, A. R., "Advances in Sonic Boom Theory, Aerodynamic Analyses Requiring Advanced Computers," Pt. II, NASA SP-347, 1975, pp. 1033-1048.

[20]Gottlieb, J. J., "Sonic Boom Research at UTIAS," *Canadian Aeronautics and Space Journal*, Vol. 20, May 1974, pp. 199-222.